Nanoscale

Accepted Manuscript

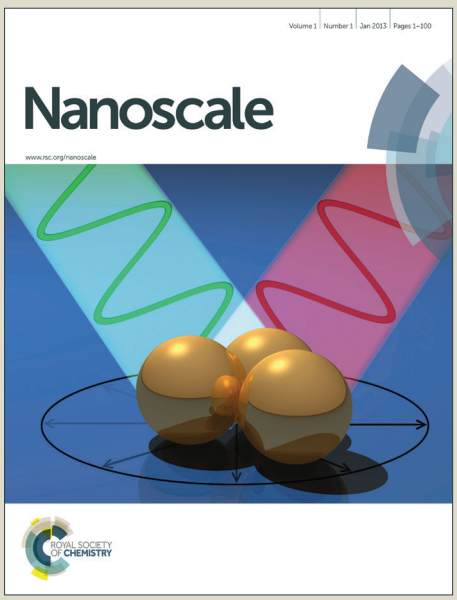

ROYAL SOCIETY OF CHEMISTRY

www.rsc.org/nanoscale

Nanoscale

RSCPublishing

COMMUNICATION

Fabrication of Graphene Nanomesh using Platinum Nano-Network as a Pattern Mask

Cite this: DOI: 10.1039/x0xx00000x

Insub Jung[a], Ho Young Jang[a], Junghyuk Moon[b] and Sungho Park[a,b,1]

Received 00th January 2012,
Accepted 00th January 2012

DOI: 10.1039/x0xx00000x

www.rsc.org/

[a]Department of Energy Science, Sungkyunkwan University, Suwon, 440-746, South Korea

[b]Department of Chemistry, Sungkyunkwan University, Suwon, 440-746, South Korea

[1]Electronic mail: spark72@skku.edu

Here, we report a facile method to fabricate graphene nanomesh (GNM) by using a platinum (Pt) metal nano-network as a pattern mask. A hexagonally ordered Pt nano-network (i.e. nanomesh) with high-density arrays of periodic nano-holes was synthesized using an anodized alumina template, which served perfectly as a pattern mask for generating GNMs with tunable pore neck widths. Altering the neck width of the pores allows the modulation of the electrical conductivity of the GNMs. Resultant GNMs were further characterized with Raman spectroscopy and their electrical properties as conducting channels in field-effect transistors (FETs) were evaluated as a function of neck width. This synthetic route for producing GNMs provides a low-cost and simple way to fabricate GNMs for use in future fundamental studies related to graphene.

Since the discovery of graphene, a single atom-thick layer of sp^2-bonded carbon atoms in a hexagonal lattice, in 2004,[1] its extraordinary properties such as high mobility,[2] transparency,[3] and flexibility[4] have been extensively studied in the fields of optics,[5] energy-related devices,[6] and electronics.[1] Specifically, graphene's high carrier mobility (up to 200,000 cm^2 V^{-1} s^{-1}) makes it a particularly promising candidate to replace Si in many applications.[7] However, the semi-metal behavior observed in graphene (i.e. zero bandgap) hinders its use in some practical applications; native graphene is not an ideal material for field-effect transistor (FET) devices due to its low on/off current ratio. These limitations have spurred a growing interest in new graphene structures and architectures to open the bandgap. These efforts include fabricating graphene nanoribbon (GNR),[8] graphene nanoring (GRNR),[9] and graphene nanomesh (GNM),[10, 11] all of which have shown semiconducting behavior due to quantum confinement effects[12] and edge roughness.[13]

In the case of GNRs, the fabrication of large-area, aligned arrays remains a major challenge.[14] Alternatively, Yusin Pak et al. [9] have successfully fabricated high-density, large-area, aligned GRNRs and have proven their ability to act as a conducting channel in a FET device, although this work remains at an early stage. Amongst all the aforementioned graphene nanostructures, one representative example is graphene nanomesh that can be thought of as many highly connected GNRs with bandgap inversely proportional to the neck width (w), the smallest distance between pores, over large area, which further can be compatible with the present thin film process. Typically, a top-down lithographic approach, combined with block copolymer nanospheres, has been used to pattern graphene into a GNM.[14, 15] However, this approach corrupts and degrades the materials due to the usage of multiple processing steps and reactive plasma gases such as CHF_3.

Recently, Zhiyuan Zeng et al.[16] demonstrated the fabrication of GNMs using anodized aluminum oxide (AAO) templates as an etching mask with the help of O_2 plasma etching. However, the presence of poly (methyl methacrylate) (PMMA) to protect the graphene from direct contact with the AAO templates complicates the process in terms of thickness control and the duration of the O_2 plasma treatment. The intrinsically isotropic nature of the O_2 plasma etching process and the relatively long pathway of the oxygen penetrating into the walls of the AAO make it difficult to achieve the desired pattern area during etching.

The typical method used to produce graphene is mechanical exfoliation from graphite flakes; this method is simple and achieves pristine graphene,[1] but it is not possible to scale up the quantity of graphene produced. Alternatively, reduced graphene oxide (rGO) provides a low-cost, easily accessible process and can be functionalized in a variety of ways.[17, 18] Moreover, this method is good for the mass production of graphene flakes. However, it cannot be used to produce a uniform layer of graphene at a large scale. In this context, chemical vapor deposition (CVD) has been commonly used for the growth of high quality graphene on metal catalysts. This method is superior to the aforementioned processes in terms of quality and scalability, both of which are essential in large-scale thin film technologies.[19, 20]

We recently reported the fabrication of a platinum (Pt) metal nano-network using an AAO template as a pattern mask, although an AAO has been known for growth of one-dimensional nanomaterials via electrochemical method.[21] The neck width of the hexagonally-ordered Pt nano-network can be tuned by varying the current or deposition time. This enables us to fabricate a pattern mask that can be used for etching. In this paper, we fabricated graphene nanomesh using a Pt nano-network as a pattern mask through simple sputtering and transferring steps with the assistance of O_2 plasma etching. This synthetic method allows us to control the neck width of our GNMs, which is important for tailoring their electronic properties.

Experiments

Synthesis of platinum (Pt) nano-network:

The detailed synthesis of our AAO has already been reported elsewhere.[22] The AAO was cut into rectangles and placed on a glass substrate. A thin film of Pt (99.99 % target purity, JEOL) was sputtered on the AAO templates using a simple sputter coater (Cressington 108 AUTO) followed by spin coating PMMA at 3500 rpm for 30 s to maintain the shape of the network. The resulting film was floated for 30 min on a solution of 3 M NaOH to dissolve the AAO template. The film was then washed several times with DI water. For FE-SEM characterization, films were transferred onto Si wafers and dipped in acetone to remove the PMMA films.

CVD growth and transfer of graphene:

Cu foils (Alpha Aesar, 75 μm, 99.999 % purity) were rinsed with HF and then washed with acetone and methanol. After blowing with N_2 gas, the Cu foils were inserted into the chamber and the temperature was increased up to 1,000 °C under H_2 (10 sccm, 100 mTorr). To remove naïve oxide films from the Cu foils and to crystallize the surface into the (111) phase, further annealing was performed for 30 min. Then, a hydrocarbon source (CH_4) was introduced and the system was kept constant for 30 min (20 sccm, 300 mTorr) in order to grow the graphene. After the decomposition of graphene onto the Cu foils, the furnace was quickly removed from the hot zone to allow for the nucleation and formation of graphene. In order to transfer the graphene onto an insulating substrate, PMMA was spin-coated onto the as-prepared graphene/Cu foils and the samples were floated on a Cu etchant ($FeCl_3$) for several hours to remove the Cu foils. Samples were then rinsed with DI water several times; the resulting films were scooped up by 300-thick SiO_2/Si wafers and dried in a vacuum chamber. Finally, the PMMA film was removed by dipping the samples in acetone and blowing them with N_2 gas.

Fabrication of graphene nanomesh (GNM):

A Pt nano-network film floated on DI water was transferred to graphene coated on a SiO_2/Si wafer. Residual PMMA films on Pt nano-network films were dissolved in acetone for 30 min. The resulting film was treated with oxygen plasma (50W power, 20 sccm) for 10 s to remove graphene from the areas unprotected by the Pt nano-network. An aqua regia solution was used overnight to etch away the Pt nano-network leaving behind the graphene nanomesh. The GNM was then washed with DI water and acetone.

Characterization of graphene nanomesh:

FE-SEM images were obtained using JEOL 7600F. Raman spectra were collected using a WITEC alpha300 with a 532 nm excitation wavelength. All the Raman spectra were performed with an exposure time of 0.5 s and measured 10 times. Electrical measurements were performed using an HP Agilent 4156 A under ambient conditions. AFM (Park systems) was conducted in non-contact mode at a scan rate of 0.28 Hz.

Results and Discussion

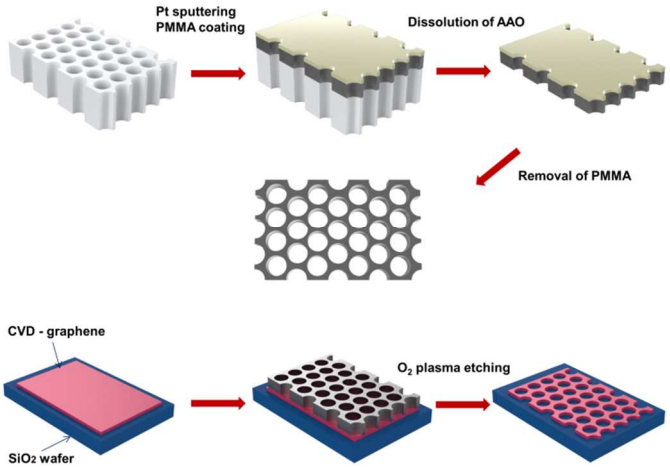

Fig. 1 Schematic illustration of the fabrication of Pt nano-network and graphene nanomesh, respectively.

Figure 1 shows a schematic illustration of the fabrication of Pt nano-networks and GNMs, respectively. The detailed synthesis of the Pt nano-network is described in the experimental section. Briefly, a thin film of Pt was sputtered on top of an AAO template with vertical arrays of nano-holes (ca. 80 nm in diameter) through simple sputtering, followed by spin coating of PMMA in order to hold the hexagonal frame of the metal network. After dissolving the AAO template in a 3M NaOH solution for 30 minutes, the film was washed by floating on deionized (DI) water. Then, substrates of as-prepared CVD-grown graphene on a 300-thick SiO_2/Si wafer were used to scoop up the floating Pt nano-network/PMMA films and the samples were dried in the oven at 80 °C. After removal of the PMMA in acetone, the sample was treated by O_2 plasma for 10 s, followed by etching of the Pt nano-network in an aqua regia solution overnight, resulting in GNM films on wafers.

Figure 2A shows an optical photograph of a fabricated GNM (2 x 2 cm^2) on a SiO_2 wafer, which is clearly visible due to the optical contrast.[23] CVD enables the fabrication of graphene at large scales since the size is only limited by the size of metal catalysts. Wafer-scale synthesis of graphene has already been demonstrated.[24]

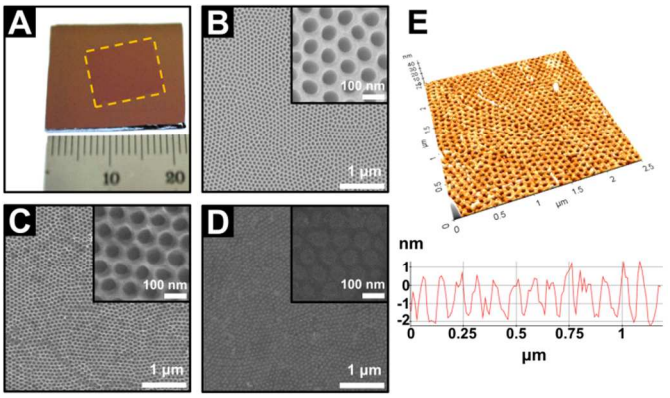

Fig. 2 (A) A photograph of fabricated GNM on SiO_2 wafer over large area. FE-SEM image of (B) an AAO template, (C) a Pt nano-network, and (D) a representative GNM film, respectively. The each inset show high-resolution images. (E) 3-D AFM image and the height profile of a GNM showing the uniform and flat film.

Similarly, the size of the Pt nano-network is only affected by the size of the AAO template as well, which implies that GNMs can be fabricated with large area since our synthetic method simply uses a combination of sputtering and a transfer step. Field-emission scanning electron microscope (FE-SEM) images of an AAO template, a Pt nano-network, and a GNM film are shown in Figures 2B-2D, respectively. Uniformly-ordered hexagonal arrays of GNMs have a high density of pores; these pores are a key factor in determining the total conductance of the film.[14] The homogeneity and roughness of the GNM were further confirmed by atomic force microscopy (AFM), as shown in Figure 2E. Both the morphology image and the height profile show the regularity and the uniformity of the final GNM films over large areas. Ideally, this synthetic approach for generating metal nano-networks could be applied to any noble metal such as Au or Ag.[25] Pt is expected to be the most desirable element as a pattern mask since it is inert and stable in harsh environments. Pt will not readily oxidize during O_2 plasma treatments, unlike other materials (e.g. Cu and Ni) which are known to easily- undergo oxidation.

Since the bandgap opening is inversely proportional to the neck width,[12] the tunable fabrication of GNM is critical not only to achieve semiconducting properties, but to potentially tailor other unprecedented properties. In this context, we fabricated Pt nano-networks with different neck widths by simply adjusting the duration of the Pt deposition time. Figures 3(A-C) show FE-SEM images of Pt nano-networks with different neck widths: 14±2, 30±3 and 36±3 nm, respectively. As we increased the sputtering time of Pt from 40 s to 60 s under a constant current level of 20 mA, neck widths increased while preserving a periodic honeycomb structure. Another advantage of using Pt as the network material for the pattern mask is its relative softness compared to the AAO. To successfully produce GNMs, it is important that the pattern mask is gently attached to the graphene so as not to damage the underlying graphene or degrade any of its properties. Figure 3A shows a wrinkle on the Pt network demonstrating the soft nature of Pt; this softness should limit the damage done to the graphene surface. Using the Pt network as a pattern mask and following the process described in Scheme 1, GNMs with controllable neck widths can be successfully replicated. Resultant GNMs with neck widths of 16±2, 29±3, and 36±4 nm are shown in Figure 3(D-F), respectively. The highly regular pattern of GNMs is clearly evident in large scale FE-SEM images, and each zoomed-in inset demonstrates the controllability of the neck width. Based on these FE-SEM images, defects or cracks in the network

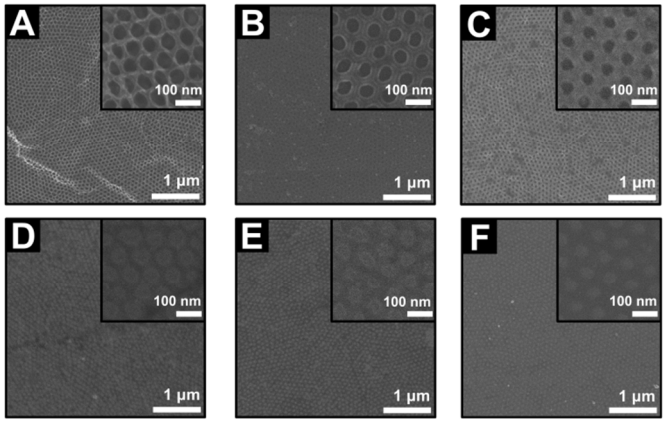

Fig. 3 FE-SEM images of Pt nano-network with different neck widths of (A) 14±2 nm, (B) 30±3 nm, and (C) 36±3 nm. FE-SEM images of GNM with different neck widths of (D) 16±2 nm, (E) 29±3 nm, and (F) 36±4 nm, by using corresponding Pt nano-network (A-C), respectively.

were not observable, indicating the high quality of our GNMs.

We characterized as-prepared GNMs systematically by Raman spectroscopy. In general, carbon materials have been well studied using Raman spectroscopy, which can provide information about the quality and the number of layers in a material.[26,27] First, the intrinsic CVD-grown graphene (black line) showed typical Raman features. A G peak (~1580 cm^{-1}) and a 2D peak (~2680 cm^{-1}), which are related to the opposite vibration of each carbon lattice and the second order vibration by phonon scattering, respectively, are shown in Figure 4A.[26] The negligible D peak (~1350 cm^{-1}), which is associated with defects, further indicates that our as-prepared graphene is high quality and is comparable to other CVD-grown graphene reported in the literature.[4, 20] When the Pt nano-network was placed on the graphene (red line), the G and 2D peaks were significantly dampened because the top Pt layer blocks light scattering from the underlying graphene layer. In addition, the D peak occurred since Pt nano-network may be considered as defects on the surface of graphene due to relatively large size of laser spot (~1 μm). Through O_2 plasma etching, we observed that all of the Raman features of graphene completely disappeared (blue line), indicating that the graphene areas that were unprotected by the Pt nano-network were etched away, leaving the hexagonally formed GNM and Pt nano-network.

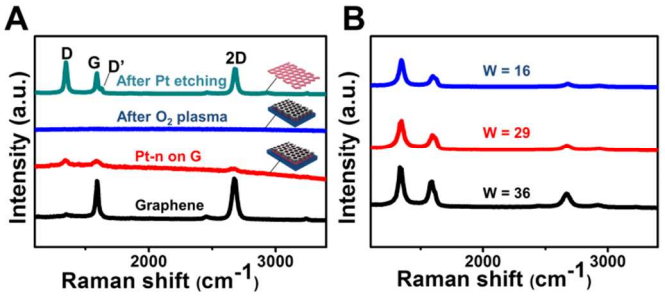

Fig. 4 (A) Raman spectra corresponding to each process of GNM. (B) Raman spectra of fabricated GNMs with different neck widths.

Finally, after removing the Pt nano-network (green line), a relatively high intensity D peak reappeared. The high intensity of the D peak in GNMs compared to graphene without the hexagonal hole arrays is

expected because the nanomesh has a large density of edges.[28] It is also noteworthy that there was an additional D' peak (~1610 cm^{-1}), which is observable when there are additional defects in the film. Slight decreases in both the G and 2D peaks in the GNM spectra, compared to those of pristine graphene, are due to shrinkage in the graphene coverage.[29] We performed more Raman spectroscopy on GNMs with different neck widths: 36 nm, 29 nm, and 16 nm, respectively (Figure 4B). Upshift of all the G peaks (1587, 1591, and 1598 cm^{-1} with decreasing the neck width) of each GNMs compared to pristine graphene (~1580 cm^{-1}) confirms increased hole doping,[30, 31] well matched with electrical measurements data that will be discussed later. The intensity ratio of the D peak (I_D) to the G peak (I_G) is a strong indication of defects in the system.[26, 32] In this case, I_D:I_G increased from 1.05 to 1.3 as neck widths decreased from 36 nm to 16 nm. This decrease is attributed to the high density of edges in GNM.[14, 31, 33] In addition, reduced intensity of 2D peak related to the mobility of films as decreasing the neck width is consistent with typically observable GNM reported in the literature.[31]

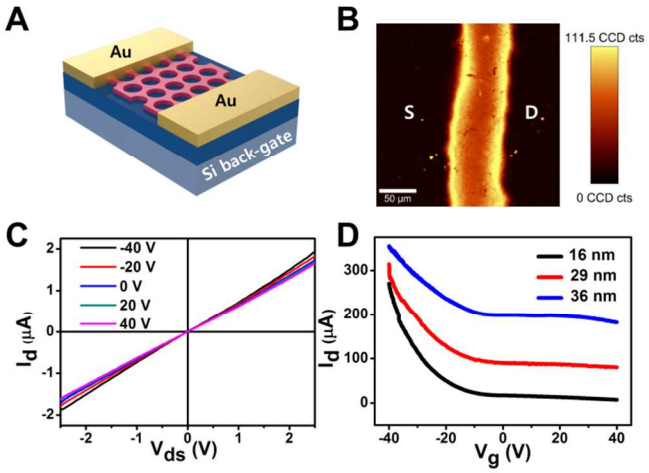

Fig. 5 (A) Schematic illustration of GNM field-effect transistor using Si wafer as a back gate. (B) 2D Raman mapping of GNM channel (C) I-V curve at different applied gate voltages from -40 V to 40 V, indicating effective modulation of GNM channel. (D) Output characteristics of fabricated GNM FETs with different neck widths at V_d = 100 mV.

As a proof of concept, we fabricated a simple GNM-based FET device in order to investigate the electronic properties of our GNM using a Si wafer as a back gate. Electrical measurements were performed under ambient conditions to gain further insight on our ability to control the neck width in our GNMs. Figure 5A is a schematic illustration of the fabricated FET device with Au electrodes. A GNM that was 50 μm long and 1 mm wide was used as the channel and a Si wafer was used as the back gate. Raman mapping of the 2D peak over the GNM channel shown in Figure 5B clearly shows a continuous, 50-μm-wide GNM channel and two Au electrodes as the source and drain. I-V characteristics shown in Figure 5C indicate that our fabricated GNM can be modulated by varying the applied voltage from -40 V to 40 V and successfully acts as a conducting channel in FET devices. We also measured output transfer characteristics of samples with 16, 29, and 36 nm neck widths (Figure 5D). All of the fabricated samples showed p-type semiconducting behavior likely due to edge oxidation or wet chemical etching.[8, 12, 14] As the neck width decreased from 36 nm to 29 nm to 16 nm, the on/off ratio of each sample was 1.95, 3.92, and 38.62, respectively, indicating enhanced semiconducting behavior as the neck width decreased. Similar results have been observed in other GNM-based FETs with a comparable size of neck width.[14, 16, 34] However, the current results clearly show that the correlation between the electronic properties and neck width of GNM is experimentally evident and there is more room to improve the measured on/off ratio by shrinking down the size of neck width. We are currently modifying the synthetic procedure to further narrow down the neck width of GNM by improving the synthetic process of metal nanoframes.

Conclusions

In summary, we reported a novel, template-assisted method that is simple and high-throughput for the fabrication of GNMs with tunable neck widths using Pt nano-networks as the pattern mask. A Pt nano-network that has a uniform, well-ordered hexagonal mesh architecture successfully served as a pattern mask when combined with oxygen plasma etching. Fabricated GNM-based FET devices showed typical p-type behavior. We also demonstrated that our strategy allows for increased control over the electronic properties of GNMs; tuning the neck width results in electrical modulation in the resultant devices. Since our method does not require any costly equipment, it is both low-cost and easily accessible. Furthermore, it provides the opportunity to achieve high on/off ratios when the neck width is reduced below 10 nm, because the quantum confinement effect can be maximized. We believe this facile method to produce GNMs not only provides a novel way to generate GNMs, but will also make it easier to study the fundamental properties of GNMs in general.

Acknowledgements

This work was supported by the National Research Foundation of Korea (National Leading Research Lab:2012R1A2A1A03670370).

Notes and references

[a] Address here.
[b] Address here.
[c] Address here.

† Footnotes should appear here. These might include comments relevant to but not central to the matter under discussion, limited experimental and spectral data, and crystallographic data.

Electronic Supplementary Information (ESI) available: [details of any supplementary information available should be included here]. See DOI: 10.1039/c000000x/

1. K. S. Novoselov, A. K. Geim, S. V. Morozov, D. Jiang, Y. Zhang, S. V. Dubonos, I. V. Grigorieva and A. A. Firsov, *Science*, 2004, **306**, 666-669.
2. A. K. Geim and K. S. Novoselov, *Nature Materials*, 2007, **6**, 183-191.
3. S. Bae, H. Kim, Y. Lee, X. F. Xu, J. S. Park, Y. Zheng, J. Balakrishnan, T. Lei, H. R. Kim, Y. I. Song, Y. J. Kim, K. S. Kim, B. Ozyilmaz, J. H. Ahn, B. H. Hong and S. Iijima, *Nat Nanotechnol*, 2010, **5**, 574-578.
4. K. S. Kim, Y. Zhao, H. Jang, S. Y. Lee, J. M. Kim, K. S. Kim, J. H. Ahn, P. Kim, J. Y. Choi and B. H. Hong, *Nature*, 2009, **457**, 706-710.

5. G. Jo, M. Choe, S. Lee, W. Park, Y. H. Kahng and T. Lee, *Nanotechnology*, 2012, **23**.
6. M. D. Stoller, S. J. Park, Y. W. Zhu, J. H. An and R. S. Ruoff, *Nano Letters*, 2008, **8**, 3498-3502.
7. K. I. Bolotin, K. J. Sikes, Z. Jiang, M. Klima, G. Fudenberg, J. Hone, P. Kim and H. L. Stormer, *Solid State Commun*, 2008, **146**, 351-355.
8. X. Li, X. Wang, L. Zhang, S. Lee and H. Dai, *Science*, 2008, **319**, 1229-1232.
9. Y. Pak, H. Jeong, K. H. Lee, H. Song, T. Kwon, J. Park, W. Park, M. S. Jeong, T. Lee, S. Seo and G. Y. Jung, *Advanced Materials*, 2013, **25**, 199-204.
10. J. W. Bai, X. Zhong, S. Jiang, Y. Huang and X. F. Duan, *Nat Nanotechnol*, 2010, **5**, 190-194.
11. O. Akhavan, *Acs Nano*, 2010, **4**, 4174-4180.
12. M. Y. Han, B. Ozyilmaz, Y. B. Zhang and P. Kim, *Physical Review Letters*, 2007, **98**.
13. D. A. Areshkin, D. Gunlycke and C. T. White, *Nano Letters*, 2007, **7**, 204-210.
14. A. Sinitskii and J. M. Tour, *Journal of the American Chemical Society*, 2010, **132**, 14730-14732.
15. M. Kim, N. S. Safron, E. Han, M. S. Arnold and P. Gopalan, *Nano Letters*, 2010, **10**, 1125-1131.
16. Z. Y. Zeng, X. Huang, Z. Y. Yin, H. Li, Y. Chen, H. Li, Q. Zhang, J. Ma, F. Boey and H. Zhang, *Advanced Materials*, 2012, **24**, 4138-4142.
17. H. L. Guo, M. Peng, Z. M. Zhu and L. N. Sun, *Nanoscale*, 2013, **5**, 9040-9048.
18. S. Park and R. S. Ruoff, *Nat Nanotechnol*, 2009, **4**, 217-224.
19. A. Ambrosi, A. Bonanni, Z. Sofer and M. Pumera, *Nanoscale*, 2013, **5**, 2379-2387.
20. X. S. Li, W. W. Cai, J. H. An, S. Kim, J. Nah, D. X. Yang, R. Piner, A. Velamakanni, I. Jung, E. Tutuc, S. K. Banerjee, L. Colombo and R. S. Ruoff, *Science*, 2009, **324**, 1312-1314.
21. H. Y. Jang, S.-K. Lee, S. H. Cho, J.-H. Ahn and S. Park, *Chem Mater*, 2013, **25**, 3535-3538.
22. H. M. Bok, K. L. Shuford, S. Kim, S. K. Kim and S. Park, *Nano Letters*, 2008, **8**, 2265-2270.
23. P. Blake, E. W. Hill, A. H. C. Neto, K. S. Novoselov, D. Jiang, R. Yang, T. J. Booth and A. K. Geim, *Appl Phys Lett*, 2007, **91**.
24. C. Y. Su, A. Y. Lu, C. Y. Wu, Y. T. Li, K. K. Liu, W. J. Zhang, S. Y. Lin, Z. Y. Juang, Y. L. Zhong, F. R. Chen and L. J. Li, *Nano Letters*, 2011, **11**, 3612-3616.
25. I. Jung, H. Y. Jang and S. Park, *Appl Phys Lett*, 2013, **103**.
26. A. C. Ferrari, J. C. Meyer, V. Scardaci, C. Casiraghi, M. Lazzeri, F. Mauri, S. Piscanec, D. Jiang, K. S. Novoselov, S. Roth and A. K. Geim, *Physical Review Letters*, 2006, **97**.
27. A. C. Ferrari, *Solid State Commun*, 2007, **143**, 47-57.
28. O. Akhavan and E. Ghaderi, *Small*, 2013, **9**, 3593-3601.
29. J. Lee, K. Kim, W. I. Park, B. H. Kim, J. H. Park, T. H. Kim, S. Bong, C. H. Kim, G. Chae, M. Jun, Y. Hwang, Y. S. Jung and S. Jeon, *Nano Lett*, 2012, **12**, 6078-6083.
30. A. Esfandiar, N. J. Kybert, E. N. Dattoli, G. H. Han, M. B. Lerner, O. Akhavan, A. Irajizad and A. T. C. Johnson, *Appl Phys Lett*, 2013, **103**.
31. M. Kim, N. S. Safron, E. Han, M. S. Arnold and P. Gopalan, *Acs Nano*, 2012, **6**, 9846-9854.
32. A. C. Ferrari and J. Robertson, *Phys Rev B*, 2000, **61**, 14095-14107.
33. N. S. Safron, A. S. Brewer and M. S. Arnold, *Small*, 2011, **7**, 492-498.
34. M. Wang, L. Fu, L. Gan, C. H. Zhang, M. Rummeli, A. Bachmatiuk, K. Huang, Y. Fang and Z. F. Liu, *Sci Rep-Uk*, 2013, **3**.

Table of contents